This manuscript has been authored in part by UT-Battelle, LLC, under contract DE-AC05-00OR22725 with the US Department of Energy (DOE). The US government retains and the publisher, by accepting the article for publication, acknowledges that the US government retains a nonexclusive, paid-up, irrevocable, worldwide license to publish or reproduce the published form of this manuscript, or allow others to do so, for US government purposes. DOE will provide public access to these results of federally sponsored research in accordance with the DOE Public Access Plan (http://energy.gov/downloads/doe-public-access-plan).

Multiple Analytical Approach to Isotopic Transport Analysis in Magnetic Fusion Devices

Jonah D. Duran,[a,*] Ezekial A. Unterberg,[b] Mike P. Zach,[b]

William R. Wampler,[c] Dmitry L. Rudakov,[d] and David C. Donovan[a]

[a] *The University of Tennessee - Knoxville, Nuclear Engineering Department*
Nuclear Engineering Building, 1412 Circle Drive, Knoxville TN 37996-1410

[b] *Oak Ridge National Laboratory*
1 Bethel Valley Rd, Oak Ridge, TN 37830

[c] *Sandia National Laboratory*
Sandia National Laboratories, New Mexico, P.O. Box 5800, Albuquerque, NM 87185

[d] *University of California San Diego*
9500 Gilman Drive, La Jolla, CA 92093-0021

*Email: jduran2@vols.utk.edu

Number of pages: 15

Number of tables: 2

Number of figures: 5

Abstract

High-Z impurities released from plasma material interactions have shown to limit the performace of fusion plasmas, and understanding these impurity transport mechanisms throughout the plasma scrape-off-layer is a major challenge. Presented herein is a study of tungsten (W) erosion and transport by uniquely measuring absolute quantities of isotopic W in order to determine the source of natural and enriched ^{182}W isotopes that have traveled throughout the tokamak discharges on the DIII-D National Fusion Facility at General Atomics. Two primary analysis methods have been implemented to characterize this W on graphite collector probes that were inserted into DIII-D's outboard midplane. Results from experiments using Rutherford backscattering spectrometry (RBS) have measued W particle areal densities down the centerline of the probes as high as 6E14 atoms/cm^2 with a detection limit of 1E12 atoms/cm^2. Laser ablation mass spectrometry (LAMS) has confirmed the elemental trends found with RBS and has provided additional insight into collector probe surface profiles. Two dimensional elemental and isotopic maps from LAMS are used to reveal new collector probe features and further refine the source of collected W. Variations in isotopic profiles and total W content are coupled to: a) the face of the probe being analyzed; b) the dimensions of the probe; and c) the plasma pulse parameters that were used during probe exposure. These results provide one-of-a-kind empirical evidence that is now being utilized for validation of tokamak impurity transport through theoretical models and in codes such as 3D-LIM and OEDGE.

Keywords — Tungsten, Isotopes, Plasma Material Interactions, DIII-D, Tokamak

I. INTRODUCTION & BACKGROUND

Core contamination of high Z impurities has been a plague on fusion energy science. As the impurity ions interact with the plasma electrons, many mechanisms cause the reduction of electron energy and therefore reduces the potential power output of the fusion reaction. Thus, the reduction of impurity ions in the plasma is imperative to the advancement of fusion as a backbone electricity source. The radiative power loss in a plasma has shown strong dependence on concentration and the atomic number of the impurity element. High-Z Tungsten (W) is the primary element of interest for this work because of its planned use in the divertor cassettes of the upcoming fusion device, ITER. The properties of W are favorable for the extreme environment that is experienced by plasma facing materials. However favorable these properties, the high energy plasma which is directed onto the W plasma facing components (PFC) often result in the erosion of the material. These eroded particles travel from the bulk of the PFC and into the boundary plasma. Once ionized, these particles follow magnetic flux tubes which eventually encounter the graphite collector probes that have been inserted into the plasma edge for this experiment. This study then focuses on bridging the gap between material erosion and core contamination through investigation of the scrape-off-layer transport of impurities.

Graphite collector probes have proven their utility in gathering such traveling particles within magnetic fusion devices for several decades [1, 2, 3, 4]. During this time, many materials have been collected and characterized with a variety of techniques [5]. The unique application of not only W, but isotopically enriched W has resulted in a new need for analysis capabilities. High sensitivity analytical techniques with fast turnaround times have been applied during this study to evaluate elemental and isotopic W content. The coupling of quantitative measurements via Rutherford backscattering spectrometry (RBS) with isotopic evaluation via inductively coupled plasma mass spectrometry (ICP-MS) has enabled unique isotopic tracer particle studies for the improvement of our understanding of material migration in the scrape-off-layer of divertor-based magnetic confinement fusion devices. This analysis was motivated by the DIII-D Metal Ring Campaign (MRC).

During the MRC at DIII-D, two sets of toroidally symmetric W coated titanium zirconium molybdenum (TZM) tile inserts were retrofit into the lower divertor of the vessel [6] as seen in the DIII-D poloidal cross-section of Figure 1a. The ring in the floor of the lower divertor was coated

with natural W where the isotopic mole-fraction abundances are 0.0012 ^{180}W, 0.2650 ^{182}W, 0.1431 ^{183}W, 0.3064 ^{184}W, and 0.2843 ^{186}W. The ring on the shelf of the lower divertor was coated with isotopically enriched ^{182}W, whose abundance fractions are <0.0005 ^{180}W, 0.9299 ^{182}W, 0.0284 ^{183}W, 0.0279 ^{184}W, and 0.0138 ^{186}W. With the two sets of metal inserts installed, the MRC utilized a triplet set of graphite collector probes near the outboard midplane of the device. Three different types of collector probes were installed at the head of a reciprocating arm so that they could be replaced with a new probe set after each unique set of plasma discharge exposures. Different diameters were chosen for the collector probes in order to compare the connection or collection length of each probe as is described in detail by Donovan et al. [7]. Each probe had a flat face directed toward the inner target direction (ITF) of the plasma as well as a face on the opposite side that was directed towards the outer target (OTF). These two facing directions are highlighted in the poloidal cross-section of Figure 1a. As seen in the collector probe subfigure, Figure 1b, A-type probes consisted of a 3 cm diameter housing with a windowed region for replaceable A-type inserts on the ITF and OTF sides. B and C-type probes were 1 and 0.5 cm respectively in diameter. Exposed collector probes were then removed from the vessel for ex-situ analysis.

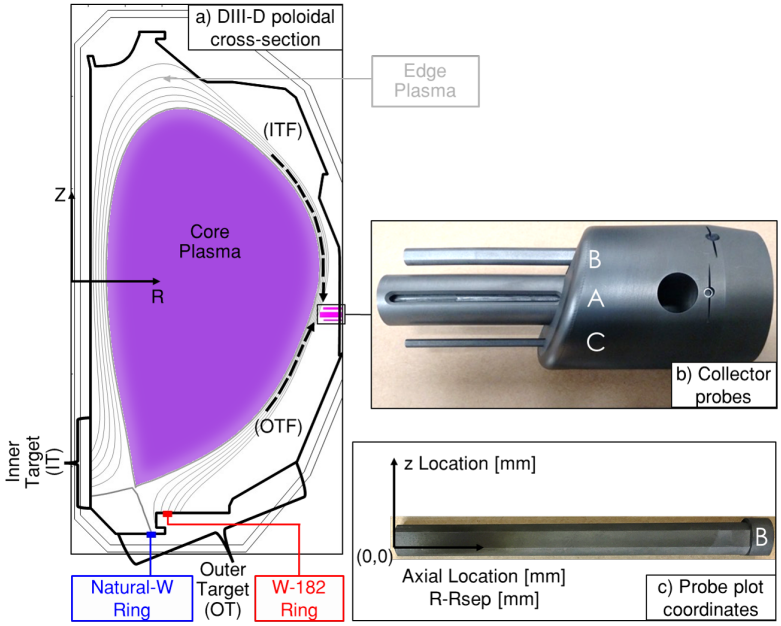

Fig. 1. DIII-D schematic of the poloidal cross section for the metal rings campaign. Inner target face (ITF) and outer target face (OTF) define the two collection surfaces for each probe in the triplet set. The coordinate systems used in the remaining figures are depicted in B-type probe overlay.

II. ANALYSIS METHODS

While there are many available methods for surface material characterization, RBS was used for its distinct ability to make non-destructive quantitative measurements of high-Z materials on low-Z substrates. Considering the MRC used low-Z rods comprised of graphite, this method is ideal for the quantification of elemental W content along the probe surface. The Sandia National Laboratory ion beam facility provided the evaluation for this study [8]. Probe measurements of W areal density (σ_W = W atoms/cm^2) were taken along 100 mm of the collection face centerline of each probe i.e., in the radial direction, in 5 mm increments. RBS parameters for the measurements are noted in Table I and described by Wampler et al. [8].

TABLE I
Ion beam analysis parameters for W areal density measurements

E [MeV]	Z1	M1 [u]	Z2	M2 [u]	Element	θ Lab [°]	θ [radian]	σ [Barn/str.]
2	2	4	74	183.85	W	165	2.88	7.3383

ICP-MS was employed for the analysis of W deposits across the surface of the collector probes, and as a destructive surface analysis technique ICP-MS followed RBS measurements. While ICP-MS allows for the mass spectrometer to receive a sample through many introduction schemes, this study focuses on an approach for direct solid sample introduction. Specifically, laser based ICP-MS techniques are employed and use a carrier gas to transfer ablated surface matter to the mass spectrometer. The union of a laser ablation tool with an ICP-MS is referred to as laser ablation inductively coupled plasma mass spectrometry (LAMS). The hardware used for this experiment includes a NewWave UP-213 nm laser ablation tool that has been plumbed to an Agilent 7700x quadrupole ICP-MS [9].

Collector probes are placed into a two-volume large format sample cell (6” x 6” x 1”) without any need for modification or sample preparation. The laser tool focuses on the surface of the probe. The ablation volume is dependent on a series of laser scan parameters as noted in Table II. The ablated aerosol resulting from a laser pulse is entrained very rapidly into a small collection cup that is positioned over the ablation site. Due to the reduced volume of the collection cup and the fixed location relative to the site of ablation, the sample collection performance of the cell is very high. Low washout time and improved gas flow dynamics are achieved relative to conventional

single volume cells. Helium carrier gas transports the ablated material to the ICP-MS torch. The sample cell is placed on a stage that is equipped with stepper motors so continuous ablation may be used at high frequencies in order to gather lines of data using time resolved analysis (TRA). During a TRA scan, a representative background is gathered before turning on the laser. There are few isobars or polyatomics that interfere with the isotopic signatures of W, and the background contribution to W mass signals is very low. This low background yields high confidence in the W measurements on the probe surface. Single centerline scans across the length of the probe are typically the focus of collector probe studies [7], but additional line scans in 0.25 mm increments across the width of the probe have provided high resolution elemental and isotopic maps of the collection surfaces. These maps offer new insights and enable the investigation of possibilities that have not previously been available in collector probe studies of large magnetic fusion energy experiments.

TABLE II
List of parameters for linear ablation scans of collector probes.

Laser λ [nm]	Scan Rate [μm/sec]	Scan Length [mm]	Pulse Rate [Hz]	Aperture Size [μm]	Energy Density [J/cm^2]
213	500	50 - 100	10	55	8

III. RESULTS AND DISCUSSION

RBS was able to measure W areal densities from 1E12 atoms/cm^2 to 6E14 atoms/cm^2, and these quantitative measurements have been essential to investigations presented in recent publications [7, 10, 11]. Normalizing the data series for a single probe allows for qualitative comparisons to normalized measurements obtained via LAMS. Both elemental W data sets have been found in good agreement with one another as seen in Figure 2.

In order to compare RBS with LAMS, an elemental signature for W is evaluated as the sum of the isotopic W intensities for a given time during the laser ablation scan. In Figure 2, W content increases with lower values of axial distance and closer position relative to the plasma separatrix (R-Rsep). At the very tip of the A-type probe insert, shadowing by the larger holder is observed as well as re-erosion of the W deposit as it is closer to the core plasma where it experiences more extreme conditions. The image of the probe insert in Figure 2 displays this shadowed region as the curved lighter portion at the left tip, and the curve is correlated to the A-type housing seen in

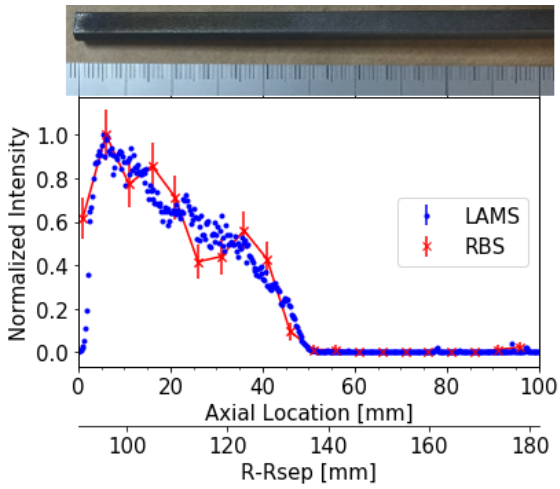

Fig. 2. RBS and LAMS elemental W intensity comparison for insert A32-OTF of shot numbers 167481-167482. These values are normalized to the maximum value in their respective series. An image of the probe insert is provided above the plot in line with the x-axes.

Figure 1b. Figure 2 displays these phenomena as well as the peak content which is at approximately 5 mm. Closer to the wall (higher R-Rsep values) from this peak, there is an exponential decrease in W content. Exponential decay is also common in collector probe studies [4, 12], and a radial decay length may be obtained with additional accuracy by fitting the LAMS data series. LAMS has the added benefit of isotopic observation, and isotopic variations across the length of the probes are presented as enrichment fractions (EF) in Figure 3. This fraction is defined as the ratio of an individual isotopic W contribution to the total elemental W signature.

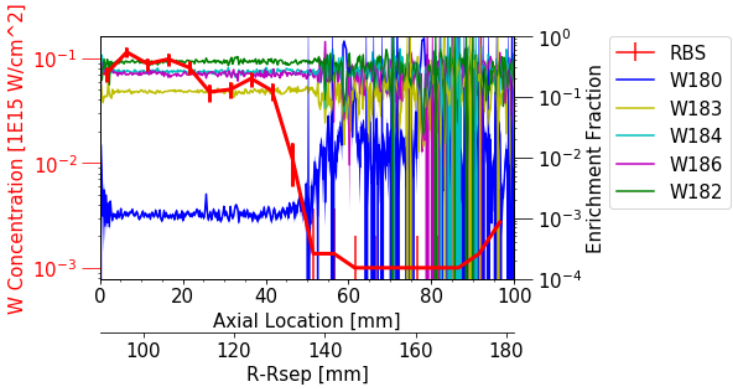

Fig. 3. Comparison of LAMS isotopic enrichment fractions and RBS areal density for probe A32-OTF of shot numbers 167481-167482. Values at 1E12 W atoms/cm^2 are at the detection limits of the technique.

To confirm EF variations on the collector probes, time-of-flight ICP-MS has been implemented [7]. Variations of ^{182}W EFs have been measured from 0.265 up to 0.9299 across a range of collector probes. This suggests W sourcing from both the natural and enriched metal rings in DIII-D. Those probes that show a higher level of enrichment indicate greater levels of W originating from the shelf metal ring of 0.9299 isotopically enriched ^{182}W. Additional isotopic measurements show that the W enrichment fractions also tend to approach a more natural abundance signature with decreasing W concentration. This has been distinctly observed to begin at 1E13 W atoms/cm^2 in Figure 3 and is common across the probe inventory. in this low concentration region, a low signal-to-noise ratio is also observed as indicated by the expansive error bands.

A series of line scans may be used in order to obtain a 2-D surface content map of the probe. 2-D surface mapping has been completed for each probe size in the triplet set as well as both of the collection surfaces that are normal to the upstream and downstream flow of the plasma. A comprehensive map of relative concentration and EF for each W isotope is provided with this method, and examples of these results are seen in Figure 4 with the coordinate system described in Figure 1c. Each colored pixel presented in Figure 4a, 4c, and 4e is a result of combining the individual isotopic W intensities into a single elemental W signature. The mass spectrometer requires 0.1 seconds to detect each W mass, so the total time to obtain an elemental W signature is therefore 0.5 seconds during the LAMS TRA scan. Combining this known integration time with the laser frequency of 10 Hz and scan rate of 0.5 mm/second, the technique delivers a total W intensity data point every 0.25 mm.

Again, the A-type probe seen in Figure 4a and 4b is an insert from a 3 cm diameter probe housing which was exposed to the plasma through a window in the holder [7]. This windowed region was seen previously in Figure 3 and is noted by the low content and low ^{182}W EF edges of the A9-OTF plots. When considering both the ITF and OTF sides of the A-type probe inserts, W content profiles display mirror like symmetry that is observed through greater W content with higher z position and lower axial position. Figure 5a shows the mirror-like symmetry through plots along the z axis for both the ITF and OTF faces of the A-type probe inserts. The faces of the probe are opposite one another, and the Z location axis follows the vessel R, Z coordinate system shown in Figure 1a such that the line of symmetry is the center of the A-type probe housing. Probes B and C were fully exposed without a housing, and the diameters of the probes were 1 cm and 0.5 cm

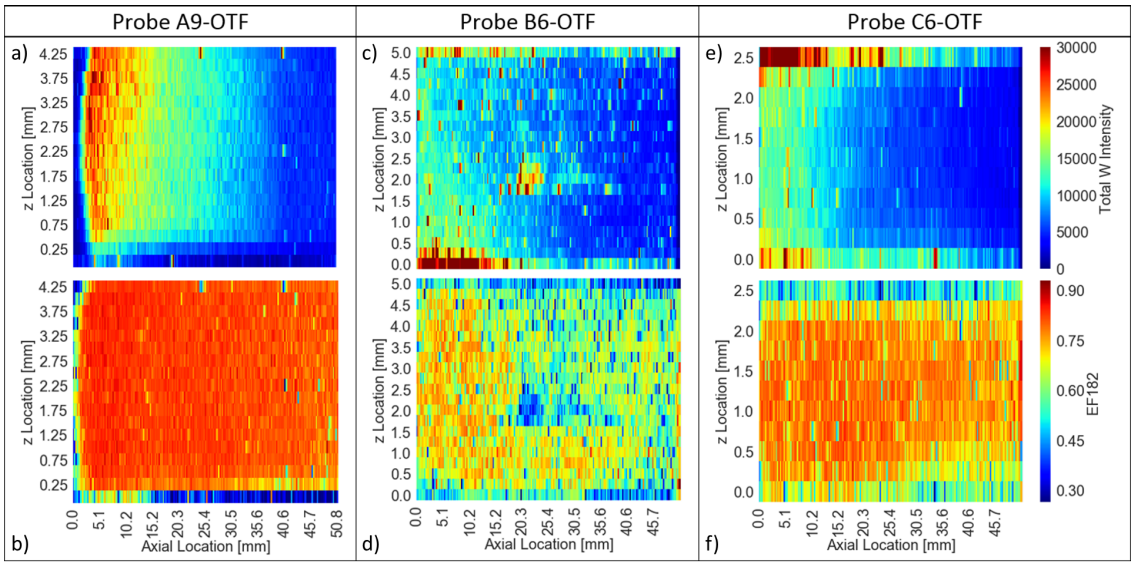

Fig. 4. Two dimensional maps of the elemental W profiles and the complementary ^{182}W enrichment fractions for the set of collector probes exposed to plasma pulses 167253-167255.

respectively. As seen in Figure 4 and Figure 5b B and C probe behavior is somewhat different than the windowed A-type probe inserts. While σ_{W} still decays exponentially past the re-erosion zone, the mapping of the probes has revealed an increase in content towards the z extremeties of the 2-D maps. This feature supports the hypothesis that the W-ions are diffusing into the flux tube of the collector probe via poloidal and radial transport processes. B6-ITF and C6-ITF of Figure 5b display the increase of edge content that is common across the B and C-type probe inventory. These "classical" profiles are of current interest to modelling efforts in an attempt to estimate the perpendicular diffusion coefficients to the probes using aforementioned impurity codes [13].

The bottom row of Figure 4 displays the complementary isotopic ^{182}W EF maps for probes A9-OTF, B6-OTF, and C6-OTF. Enrichment fractions are displayed with colorbar extremeties starting with natural 0.265 isotopic abundance levels and reaching up to 0.9299. Variations in EFs and the aforementioned total W content are coupled to the dimensions of the probe as well as the plasma pulse parameters that were used during probe exposure. For example, the A-type probe inserts display more consistent levels of ^{182}W across the scanned regions while type B and C probes show a spectrum of enrichment fractions on the collection surfaces. Probes B6-OTF and C6-OTF reveal that the higher levels of W at the z edges of the probe tend to be weighted towards a more natural ^{182}W signature, i.e. lower ^{182}W EF values.

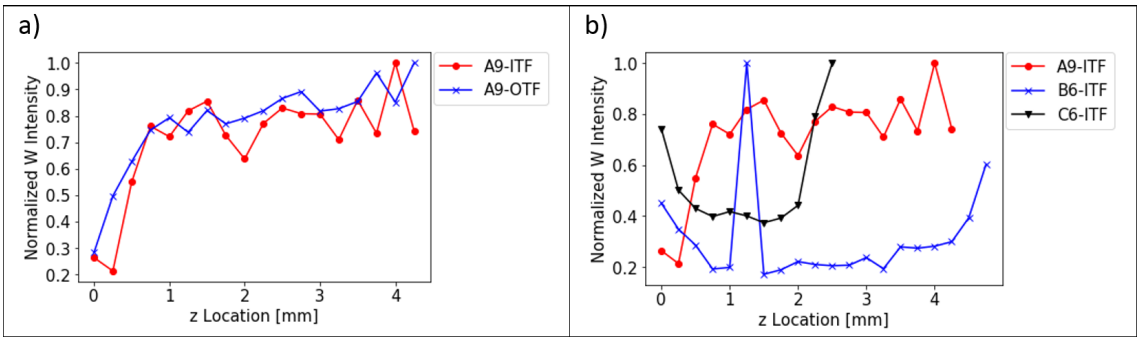

Fig. 5. The following plots are for the set of collector probes exposed to plasma pulses 167253-167255 across axial positions of ∼10 mm: a) Representative mirror-like width profiles observed across A9-ITF and A9-OTF; b) Full ITF A, B, and C-type probe width comparison displaying "classical" width profiles for type B and C probes with a typical A-type probe insert width profile. Error bars are smaller than the symbol size.

IV. CONCLUSION

The use of high-Z isotopes for tracer particle experiments during the DIII-D metal ring campaign has required the development of new methods and techniques. RBS and LAMS have offered a complementary analytical approach for the surface characterization of collector probes inserted into scrape-off-layer plasma. Empirical results from these two methods have been found in good agreement between one another and have provided quantitative measurements of W areal density along the flat face surface of the probe sets as well as isotopic identification of the various W masses which were installed into the lower divertor. These results may be used to determine how eroded divertor W is traveling as well as differentiate from which metal ring the impurities are derived. Characterization has particularly enabled studies that look into the scrape-off-layer portion of the impurity chain in order to bridge the gap between erosion of plasma facing components that may lead to core contamination. High resolution surface content maps from LAMS have also revealed new surface content features that are now motivating the validation of tokamak impurity transport through theoretical models and in codes such as 3D-LIM. In the future, these methods will also enable any additional metal ring campaigns and may be expanded to other studies of high-Z isotopic tracer studies.

ACKNOWLEDGMENTS

The authors would like to recognize support by the U.S. Department of Energy under DE-SC0016318 (UTK), DE-AC05-00OR22725 (ORNL), and DE-SC0014664 (ORAU). This material is also based upon work supported by the U.S. Department of Energy, Office of Science, Office of Fusion Energy Sciences, using the DIII-D National Fusion Facility, a DOE Office of Science user facility, under award DE-FC02-04ER54698. Additional recognition is given to Sandia National Laboratories which is a multimission laboratory managed and operated by National Technology & Engineering Solutions of Sandia, LLC, a wholly owned subsidiary of Honeywell International Inc., for the U.S. Department of Energys National Nuclear Security Administration under contract DE-NA0003525.

REFERENCES

[1] P. C. Stangeby, "Interpretation of plasma impurity deposition probes. Analytic approximation," *The Physics of Fluids*, **30**, *10*, 3262 (1987); 10.1063/1.866502.

[2] S. Cohen, "Tokamak plasma diagnosis by surface physics techniques," *Journal of Nuclear Materials*, **76-77**, 68 (1978); https://doi.org/10.1016/0022-3115(78)90120-4.

[3] D. Hildebrandt, H. Wolff, J. Roth, R. Brakel, P. Grigull, F. Rau, F. Sardei, and E. Taglauer, "Impurity collection in the SOL plasma and at the wall of W7-AS," *Journal of Nuclear Materials*, **196-198**, 436 (1992); https://doi.org/10.1016/S0022-3115(06)80074-7., plasma-Surface Interactions in Controlled Fusion Devices.

[4] W. Schustereder, K. Krieger, A. Herrmann, and V. Rohde, "Discharge resolved impurity flux measurements in the edge plasma of ASDEX Upgrade by exposure of collector probes," *Journal of Nuclear Materials*, **363-365**, 242 (2007); https://doi.org/10.1016/j.jnucmat.2007.01.011., plasma-Surface Interactions-17.

[5] A. Weckmann, "Material migration in tokamaks : Erosion-deposition patterns and transport processes," PhD Thesis, KTH, Fusion Plasma Physics (2017)QC 20170630.

[6] K. Holtrop, D. Buchenauer, C. Chrobak, C. Murphy, R. Nygren, E. Unterberg, and M. Zach, "The Design and Use of Tungsten Coated TZM Molybdenum Tile Inserts in the DIII-D Tokamak Divertor," *Fusion Science and Technology*, **72**, *4*, 634 (2017); 10.1080/15361055.2017.1347456.

[7] D. C. Donovan, E. A. Unterberg, P. C. Stangeby, S. Zamperini, J. D. Auxier, D. L. Rudakov, W. R. Wampler, M. Zach, T. Abrams, J. D. Duran, J. D. Elder, and A. L. Neff, "Utilization of outer-midplane collector probes with isotopically enriched tungsten tracer particles for impurity transport studies in the scrape-off layer of DIII-D (invited)," *Review of Scientific Instruments*, **89**, *10*, 10I115 (2018); 10.1063/1.5039347.

[8] W. R. Wampler, D. L. Rudakov, J. G. Watkins, A. G. McLean, E. A. Unterberg, and P. C. Stangeby, "Measurements of tungsten migration in the DIII-D divertor," *Physica Scripta*, **2017**, *T170*, 014041 (2017).

[9] A. L. Gray, "Solid sample introduction by laser ablation for inductively coupled plasma source mass spectrometry," *Analyst*, **110**, 551 (1985); 10.1039/AN9851000551.

[10] S. Zamperini, D. Donovan, E. Unterberg, P. Stangeby, J. Nichols, J. Duran, D. Elder, A. Neff, D. Rudakov, and M. Zach, "Transport of tungsten to collector probes in DIII-D," *Nuclear Materials and Energy*, **18**, 87 (2019); https://doi.org/10.1016/j.nme.2018.12.013.

[11] E. Unterberg, D. Donovan, J. Duran, P. Stangeby, S. Zamperini, T. Abrams, D. Rudakov, W. Wampler, and M. Zach, "Use of isotopic tungsten tracers and a stable-isotope-mixing model to characterize divertor source location in the DIII-D metal rings campaign," *Nuclear Materials and Energy*, **19**, 358 (2019); https://doi.org/10.1016/j.nme.2019.02.028.

[12] G. Staudenmaier, P. Staib, and S. Rossnagel, "Impurity transport in the ASDEX edge plasma studied by a combination of passive and active probes with SIMS analysis," *Journal of Nuclear Materials*, **111-112**, 23 (1982); https://doi.org/10.1016/0022-3115(82)90175-1.

[13] J. Elder, P. Stangeby, E. Unterberg, T. Abrams, J. Boedo, D. Donovan, A. McLean, D. Rudakov, W. Wampler, and J. Watkins, "Evidence of near-SOL tungsten accumulation using a far-SOL collector probe array and OEDGE modelling in the DIII-D metal rings L-mode discharges," *Nuclear Materials and Energy*, **19**, 287 (2019); https://doi.org/10.1016/j.nme.2019.03.007.

DISCLAIMER

This report was prepared as an account of work sponsored by an agency of the United States Government. Neither the United States Government nor any agency thereof, nor any of their employees, makes any warranty, express or implied, or assumes any legal liability or responsibility for the accuracy, completeness, or usefulness of any information, apparatus, product, or process disclosed, or represents that its use would not infringe privately owned rights. Reference herein to any specific commercial product, process, or service by trade name, trademark, manufacturer, or otherwise, does not necessarily constitute or imply its endorsement, recommendation, or favoring by the United States Government or any agency thereof. The views and opinions of authors expressed herein do not necessarily state or reflect those of the United States Government or any agency thereof.

Click here to access/download;Figure;FST18-350R1Fig1-tiff.tiff

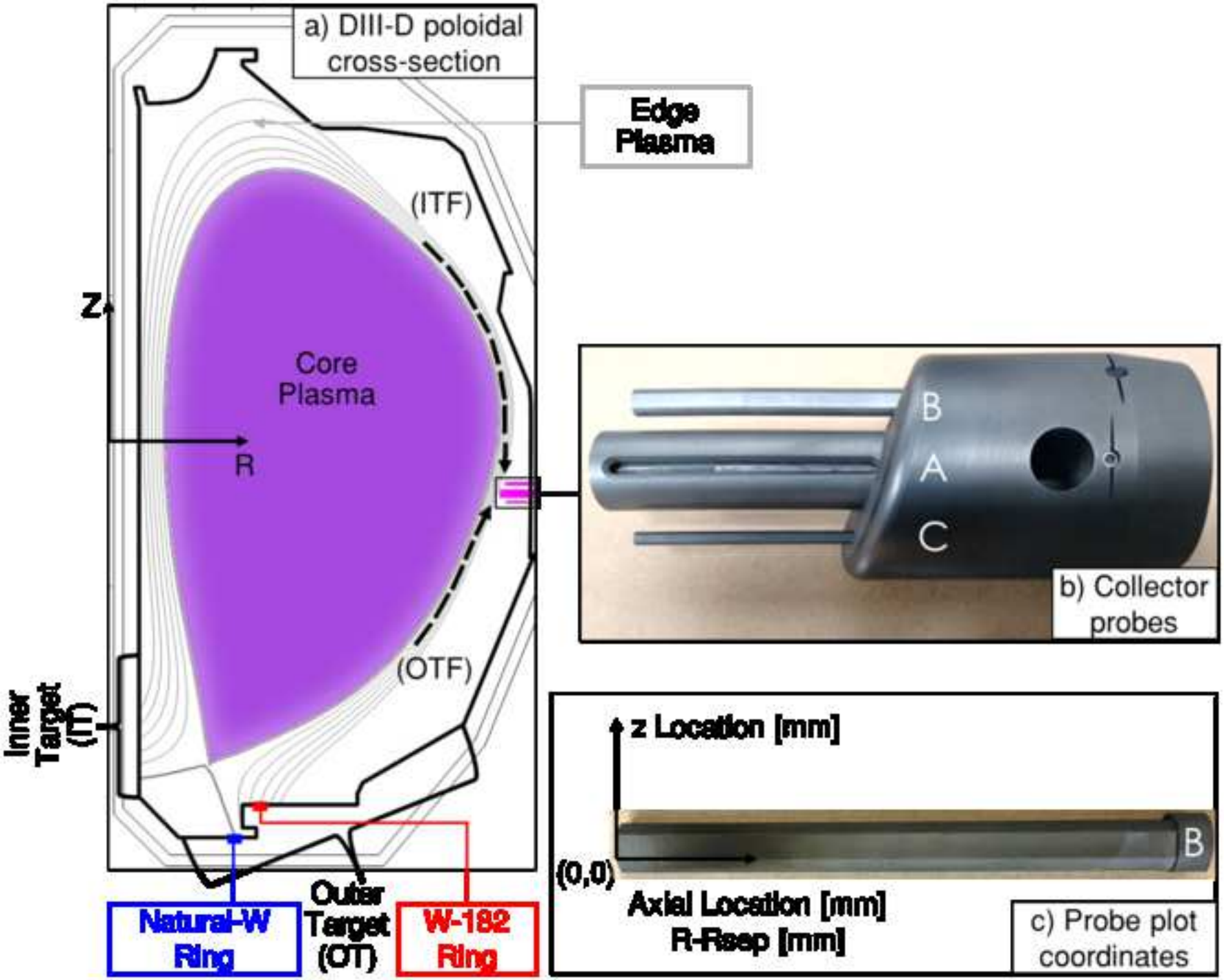

Click here to access/download;Figure;FST18-350R1Fig2-tiff.tiff

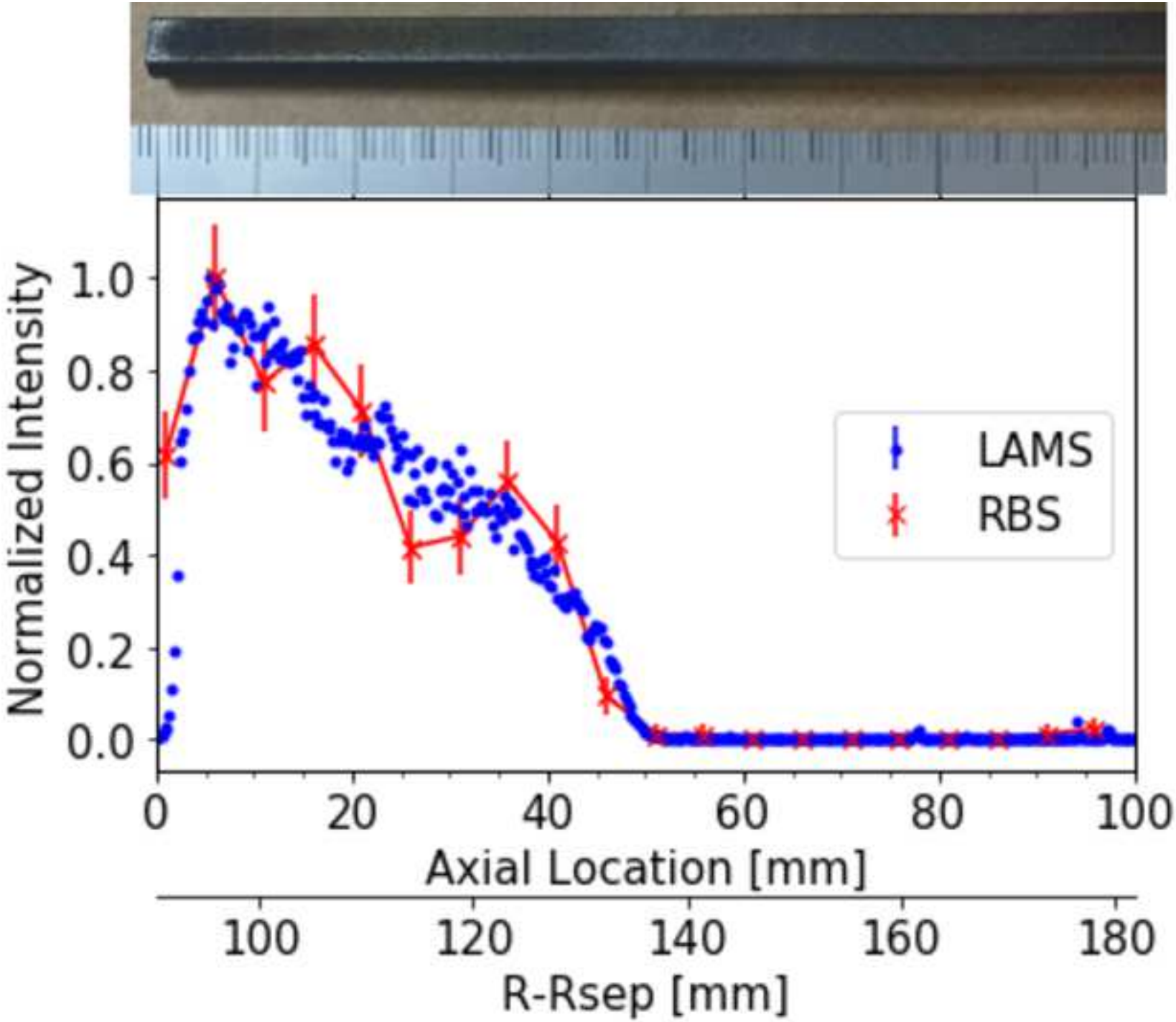

Click here to access/download;Figure;FST18-350R1Fig3-tiff.tiff

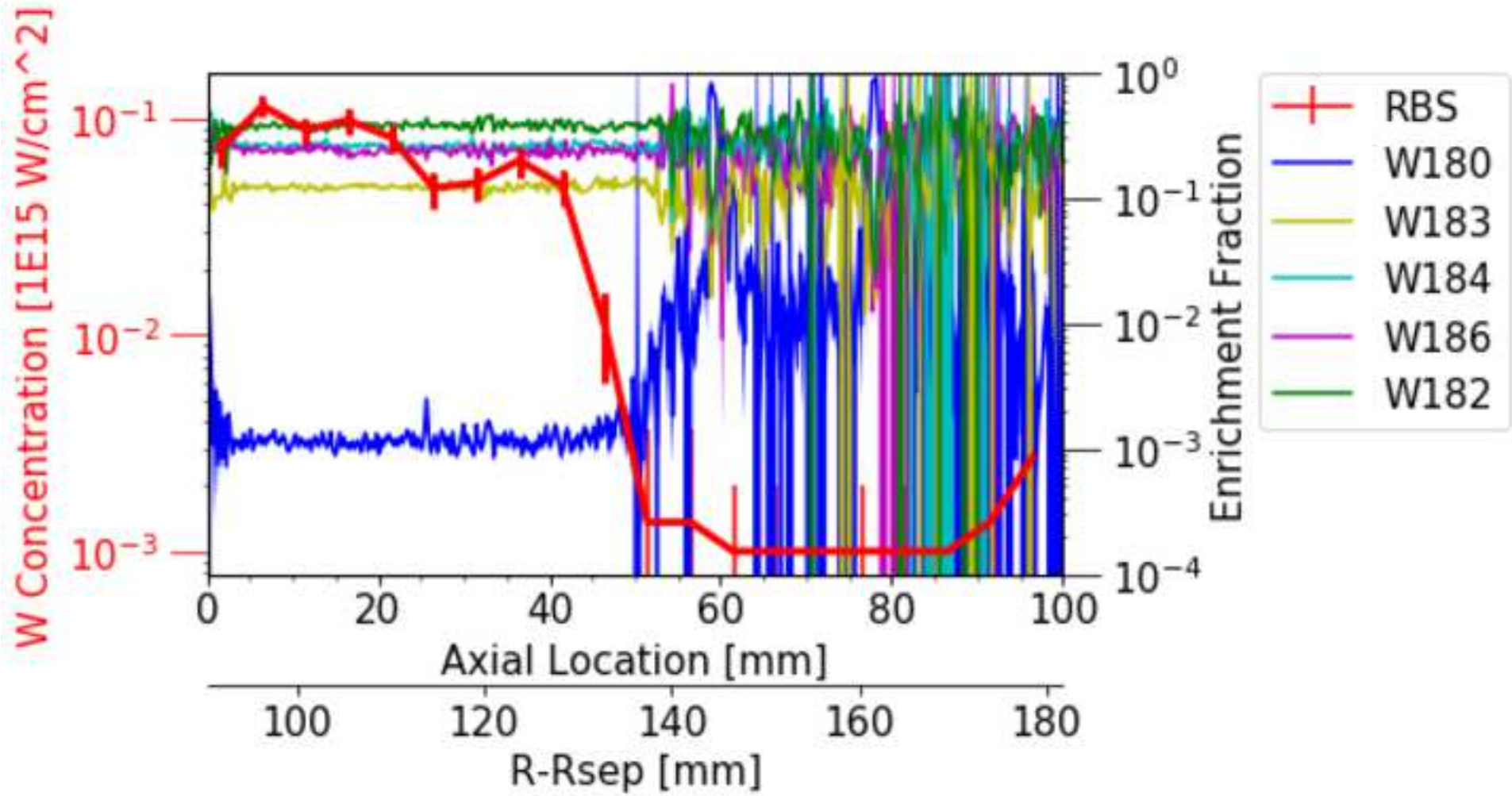

Click here to access/download;Figure;FST18-350R1Fig4-tiff.tiff

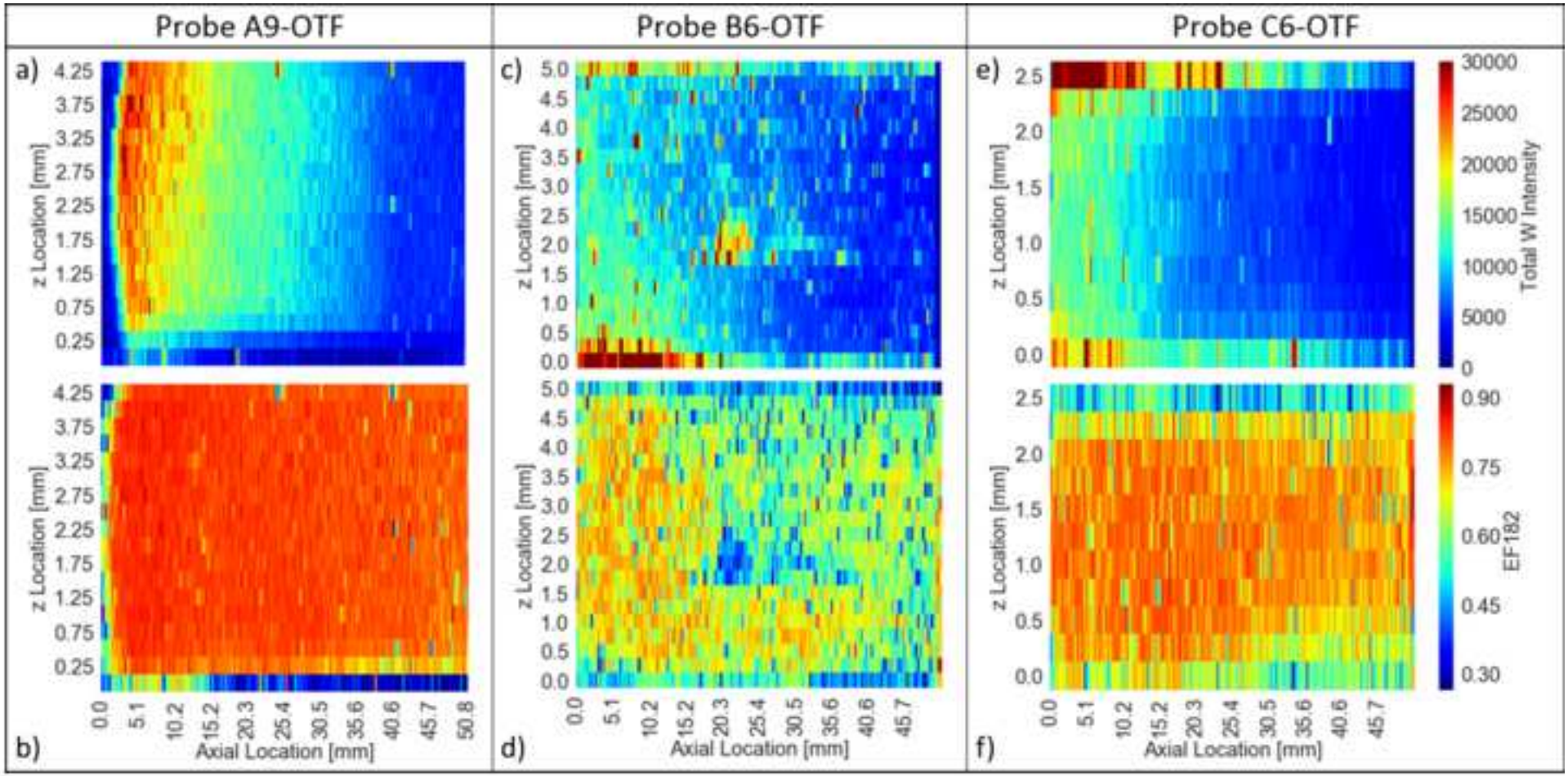
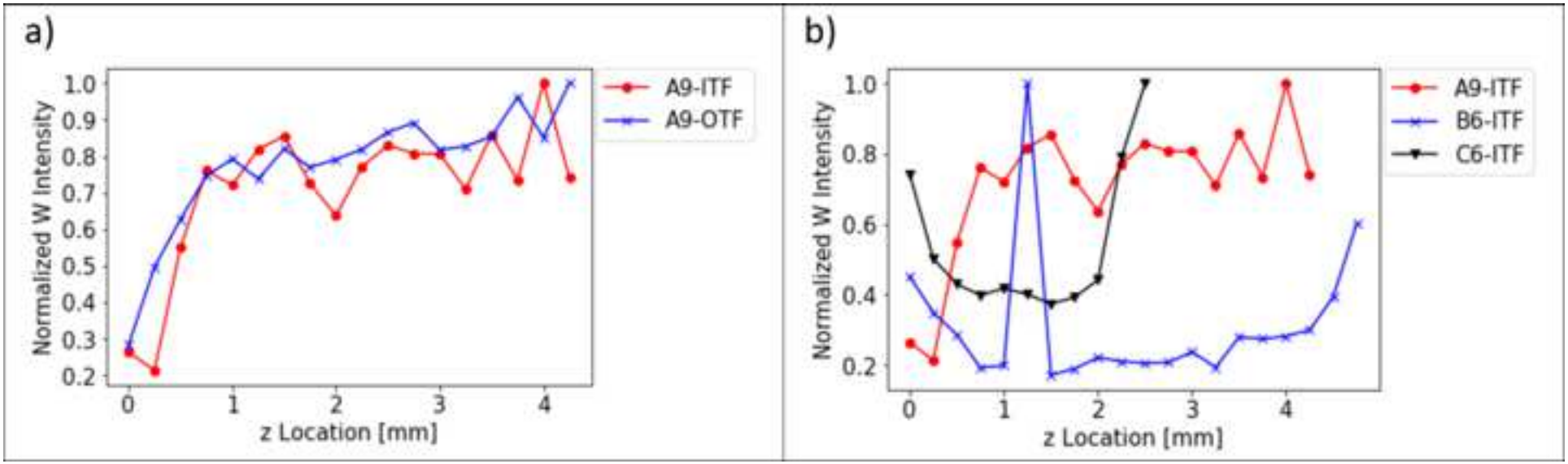
Click here to access/download;Figure;FST18-350R1Fig5-tiff.tiff